

Co-nonsolvency Transition in Polymer Solutions: A Simulation Study

Zahra Mohammadyarloo* and Jens-Uwe Sommer*

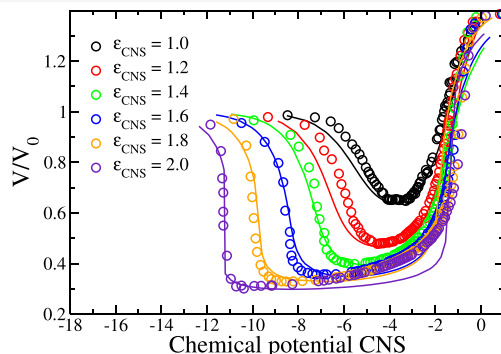
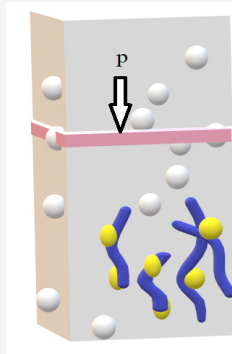
Cite This: <https://doi.org/10.1021/acs.macromol.2c01280>

Read Online

ACCESS |

Metrics & More

Article Recommendations



ABSTRACT: We study the phase segregation in polymer solutions in the presence of a co-nonsolvent (CNS) using molecular dynamics simulations, where CNS particles are a preferential solvent for the polymers. To investigate the condensation transition, we use a movable wall that exerts an osmotic pressure on the polymers but is permeable with respect to the CNS. We focus on the semidilute state of the polymer solution in the absence of CNS. Increasing the amount of CNS results in a condensation of the polymer–CNS phase, which is related to a sharp drop of the polymer volume, followed by a re-entry behavior at higher concentrations of CNS. Simulation results for different interaction energies between monomers and CNS particles are compared with the prediction of the adsorption–attraction mean-field theory under constant osmotic pressure. By calculating the radius of gyration and the structure factor of the individual chains, we found that the conformation statistics of the chains is consistent with the behavior in semidilute solution at the given concentration, resulting from the co-nonsolvency response. Concerning the diffusion dynamics of the polymer chains, we found a monotonous slowing down with increasing CNS concentration and no indication for network-like dynamics or exceptional slow dynamics at the condensation point. Our results are consistent with the collective nature of the co-nonsolvency transition due to weak and transient monomer–CNS–monomer bridging which can be rationalized using mean-field-like concepts.

1. INTRODUCTION

In their seminal work, Winnik, Ringsdorf, and Venzmer¹ have shown that a mixture of methanol and water, both known as good solvents for poly(*N*-isopropylacrylamide) (PNiPAAm), results in phase separation between the polymer and solvent well below the LCST transition, which has been termed co-nonsolvency. While PNiPAAm is the most intensively studied system for the co-nonsolvency effect,² many other polymer/solvent/cosolvent systems are known to display the co-nonsolvency effect (see for instance refs 3–6). To explain the collapse and re-entrant behavior of PNiPAAm/water/methanol, the preferential adsorption of methanol on the basis of competitive hydrogen bonds has been proposed by Tanaka et al. in refs 7 and 8. This model can be considered as an extension of their theory to explain the LCST behavior of polymer/water systems.⁹ To understand the co-nonsolvency effect in a generic way, motivated by atomistic simulations,¹⁰ Mukherji, Kremer, and Marques proposed the concept of

cosolvent-induced bridging interactions between monomers, which quantitatively explains the collapse of a single polymer chain due to the undersaturation of monomers with the preferred solvent.^{11,12} This concept can be directly transferred to coarse-grained simulation models and is not restricted to water-soluble polymers and hydrogen-bonding interactions.^{11,13} It is interesting to note that on this level of understanding of the co-nonsolvency effect there exist striking similarities to the collapse of brushlike polymers in the presence of attractive nanoparticles, which in turn mimics the gating function of the nuclear pore complex in living cells.^{14,15}

Received: June 20, 2022

Revised: August 18, 2022

Moreover, preferential and nonspecific binding of proteins to RNA and DNA may also explain the formation of protein condensates¹⁶ as well as aspects of heterochromatin formation in eukaryotic cells.^{17,18} Alternatively to the concept of preferential solubility, a strong attraction between the two solvents can lead to a demixing scenario between polymer and the two solvents.¹⁹ Other qualitative or semianalytical models for co-nonsolvency address aspects of specific systems such as methanol–water mixtures.²⁰ For a recent review of co-nonsolvency, we refer the reader to ref 21.

On the basis of the idea of preferential adsorption, the concept of the adsorption–attraction model has been developed by one of the authors and applied to polymer brushes and solutions.^{22,23} Using a mean-field approach, the bridging-induced attraction by the cosolvent or cosolute can be analytically mapped into a concentration-dependent Flory parameter, $\chi(c)$, which increases with concentration of the polymer, c , and in turn gives rise to a type II transition scenario, where the phase transition is driven by a change of sign of higher-order virial coefficients.²⁴ As a consequence, a discontinuous phase transition can be predicted even in the absence of translational entropy, i.e., in immobilized polymers and at concentrations well above the overlap threshold. This model can further explain the jumplike response of polymer brushes at the co-nonsolvency transition which can give rise to extraordinary adhesion and friction properties of polymer-coated surfaces.^{25,26}

Detailed predictions of this model have been verified in coarse-grained computer simulations following refs 11 and 13 using the Kremer–Grest model for dense polymer brushes of various grafting densities and using different sizes of the cosolvents.²⁷ This study also reveals another aspect as predicted earlier for the type II collapse transitions in polymer brushes,²⁸ namely, the coexistence of two layers in the transition range: a collapsed layer near the substrate and a swollen layer expanding into the solvent phase. It is worth noting that phase transitions and coexistence in immobilized and strongly overlapping polymers cannot be explained using the standard Flory–Huggins model where the second virial coefficient is changing sign at the theta point but requires a negative higher virial coefficient, which is a core feature of the adsorption–attraction model.²² Recently, in a series of experimental works, Yong et al. have studied the co-nonsolvency response of PNIPAAm brushes and a wide variation of parameters including a series of alcohols as cosolvents ranging from methanol to butanol, indicating the role of preferential adsorption.⁶ In addition, the adsorption–attraction model has been extended to include thermal solvent properties as well as the size of the cosolvent which led to a quantitative prediction of the PNIPAAm brush response to various alcohol–water mixtures.²⁹

So far the behavior of polymer solutions in solvent/cosolvent mixtures has not received much attention in simulation. As predicted from the adsorption–attraction model also semidilute solutions should display a discontinuous liquid–liquid phase transition triggered by the cosolvent–polymer attraction. This is in strong contrast to segregation of polymers from a single solvent in which case a high dilution of polymers well below the overlap transition is a prerequisite for coexistence.^{30,31} This is due to the fact that the low translational entropy of the macromolecules has to compete with the attraction between all monomers in the condensed state. Thus, the detection of a liquid–liquid phase transition in

semidilute polymer solutions would be another proof of concept for the type II transition scenario under co-nonsolvency.

In this work the co-nonsolvency response of a polymer solution in equilibrium has been studied using coarse-grained molecular dynamics simulations, and the results have been compared with the adsorption–attraction model. In particular, we used a simulation setup with a semipermeable wall, which generates a constant osmotic pressure for the polymers and accounts for the drastic volume shrinkage of the polymer phase during the transition. The density response of the polymer with respect to the cosolvent volume fraction is evaluated and quantitatively compared with the adsorption–attraction model. Furthermore, we investigate conformation properties of individual chains as well as their dynamical behavior at various stages of the co-nonsolvency transition. The rest of this work is structured as follows: In section 2 we describe the theoretical model and the simulation setup in detail. The results of our simulations in comparison with theory are presented in section 3, while our conclusions are given in section 4.

2. THEORY AND METHODS

2.1. Adsorption–Attraction Model for Polymer Solutions.

In this section we briefly review the adsorption–attraction model which has been developed recently in ref 23 for polymer solutions in the presence of cononsolvent (CNS). Its conceptional features are sketched in Figure 1. While the

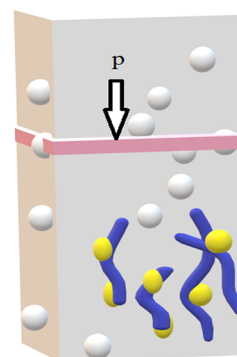


Figure 1. Sketch of the model for polymers in solution (blue color) under osmotic pressure (p) in the presence of CNS (spheres) and implicit solvent (background). A semipermeable movable wall (pink color) imposes the constant osmotic pressure onto the polymer phase. CNS and solvent can be freely exchanged. CNS particles that are adsorbed on polymers are shown as yellow spheres.

polymers are under a constant osmotic pressure, p , CNS particles are interchanged freely with a reservoir of bulk CNS concentration ρ . The chemical potential of the CNS is approximated by the lattice gas equation of state as

$$\mu = \ln\left(\frac{\rho}{1 - \rho}\right) \quad (1)$$

In the following, free energies are considered per monomer unit because the number of monomers is conserved. For simplicity, energy units are expressed in $k_B T$. Here, k_B is the Boltzmann constant and T denotes the absolute temperature. We consider no interaction between the polymers apart from excluded volume, and the two solvent species are also fully miscible. The preferential solubility of the polymer in the CNS is expressed by an energy gain, ϵ , upon contact with a

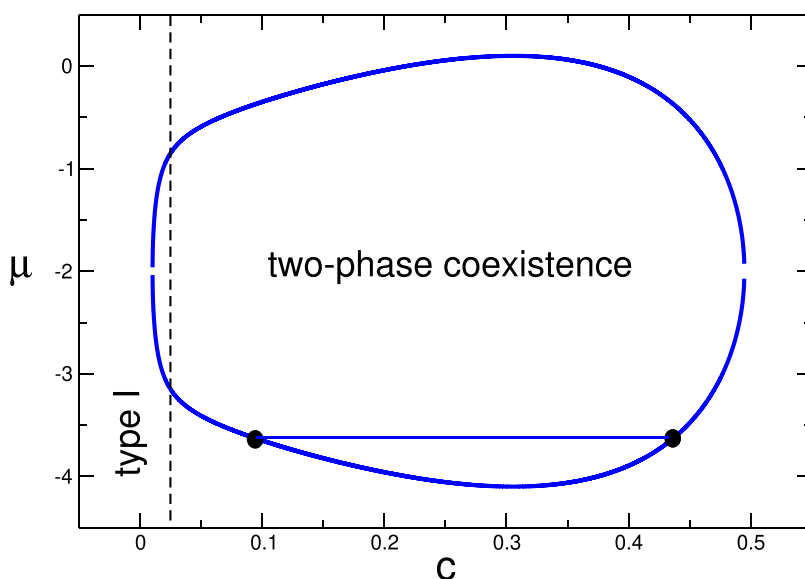


Figure 2. Example for the spinodal phase diagram of the symmetric model ($v = 0$) for $N = 100$ and $e = 2$. The phase diagram is constructed with respect to the polymer concentration, c , and the chemical potential of the CNS, μ . In the case of an ideal CNS solution this can be related to the CNS volume fraction, ρ , by $\mu = \ln\left(\frac{\rho}{1-\rho}\right)$. For very low polymer volume fractions in the diluted state the model predicts a phase transition driven by a negative second virial coefficient (type I), which corresponds to an effective poor solvent condition induced by the CNS coupling (region left of the dashed line). Notably, a discontinuous phase transition is predicted for higher concentrations, too; see the example of a spinodal tie line indicated in the plot, where the second virial coefficient is positive and the transition is driven by a negative third virial coefficient (type II). For more details, see ref 23.

monomer. We note that e might contain entropic contributions such as depletion forces.²¹ Because the co-nonsolvency transition occurs at a constant temperature, the different physical origins of e are not essential. In total, the free energy per monomer unit can be written as a sum of three contributions:

$$f = f_{\text{ads}} + f_{\text{attr}} + f_{\text{sol}} \quad (2)$$

The first term describes the adsorption of the CNS on the polymer chain

$$f_{\text{ads}} = \phi \ln \phi + (1 - \phi) \ln(1 - \phi) - \mu\phi - \epsilon\phi \quad (3)$$

where the fraction of CNS particles adsorbed or bound to the polymers per monomer unit is denoted by ϕ . Thus, ϕ is an adsorption order parameter, and the polymers play the role of the substrate for adsorption of CNS. We define the maximum adsorbed state (polymer is fully covered by CNS) as $\phi = 1$. The probability that a monomer is not occupied by CNS is then given by $1 - \phi$. The minimum of eq 3 with respect to ϕ thus defines the adsorption isotherm of the CNS on the polymer. The key argument of the adsorption–attraction model is the coupling effect caused by a “sandwich-like” simultaneous adsorption of CNS between two monomers, which reflects the original idea of the bridging effect of CNS in ref 11. This is modeled in a mean-field approximation by

$$f_{\text{attr}} = -2\epsilon\gamma\phi(1 - \phi)c \quad (4)$$

This term is rationalized as follows: the probability of finding some other monomer in the close proximity of the given monomer is defined by the volume fraction, c , of the monomers. The probability for coupling between the two monomers by a cosolvent molecule is then given by the probability that only one of the two monomers carries a CNS times the probability for a spatial contact of the monomers,

$2\phi(1 - \phi)c$. The symbol γ denotes a possible difference between the strength of the additional binding as compared to the simple binding. In all what follows we consider the case $\gamma = 1$. This means that the attraction of the CNS is not changed if the molecule has already a contact with the polymer. The free energy per monomer of the polymer solution at constant osmotic pressure is given by

$$f_{\text{sol}} = \frac{1}{N} \ln c + \left(\frac{1}{c} - 1 - v\phi \right) \ln(1 - c - v\phi c) + \frac{p}{c} \quad (5)$$

Here N denotes the degree of polymerization (number of monomers per chain), and we assume the monomer size to be equal to the size of the solvent for simplicity. This expression corresponds to the Flory–Huggins model of an athermal polymer solution. Here, we take into account the fact that the excluded volume (effective volume fraction) of the monomers is increased by adsorbed CNS, where v denotes the additional excluded volume per adsorbed unit. The case of $v = 0$ yields a symmetric solution for the equilibrium state around the point $\mu + \epsilon = 0$. This case has been treated analytically in ref 23. Most importantly we have predicted a type II discontinuous demixing transition in the semidilute regime of the polymer solution due to the CNS effect. This is in marked contrast to demixing in the two-component model which takes place at very low polymer volume fractions, typically of the order of $1/N$. In Figure 2 we display an example for the spinodal phase diagram of the symmetric model, $v = 0$, as predicted in our previous work.²³ For polymer concentrations in a highly diluted state, the CNS effect can induce an effective negative second virial coefficient related to a standard demixing transition (type I). Most interesting is the case of a semidilute solution, where the transition is driven by a negative third virial coefficient. Therefore, in the present work, we will focus on the

semidilute regime of the polymer solution to test the theoretical prediction for the CNS-driven transition.

For the general case of $\nu > 0$, only numerical solutions can be obtained. Here, we minimize the total free energy $f(\phi, c)$ with respect to both arguments—the bound CNS (ϕ) and the volume fraction of polymer (c)—which provides the equilibrium equation of state for the polymer, $c(p, \mu, \epsilon)$. In this work, we use the “fminsearch” function of MATLAB which can solve unconstrained multivariable functions using a gradient-free method. To compare with the simulation results, we use normalized values of the density with respect to the same parameters in the absence of CNS.

2.2. Simulation Method and Model Parameters. The simulations are based on the coarse-grained bead–spring molecular dynamics simulation method introduced by Kremer and Grest.^{32,33} The simulation approach follows our previous work on the co-nonsolvency response of polymer brushes.²⁷ We use an explicit CNS but implicit common solvent model. The interactions of all particles are modeled via a truncated and shifted Lennard-Jones (LJ) potential with the interaction energy of ϵ_{LJ} and the particle size of σ according to

$$U_{\text{LJ}}(r) = \begin{cases} 4\epsilon_{\text{LJ}} \left\{ \left(\frac{\sigma}{r} \right)^{12} - \left(\frac{\sigma}{r} \right)^6 - \left(\frac{\sigma}{r_c} \right)^{12} + \left(\frac{\sigma}{r_c} \right)^6 \right\} & \text{if } r < r_c \\ 0 & \text{if } r \geq r_c \end{cases} \quad (6)$$

All parameters are expressed in terms of LJ units: energy, ϵ_{LJ} , size of the LJ beads, σ , and mass, m , of the beads. We choose the size of the CNS particle σ_{CNS} equal to the monomer size σ_m , i.e. $\sigma_{\text{CNS}} = \sigma_m = \sigma$. The time unit is given by $\tau = \sigma \sqrt{m/\epsilon_{\text{LJ}}}$. Monomers in the polymer chain are connected by a finitely extensible nonlinear elastic potential (FENE):

$$U(r) = \begin{cases} -\frac{1}{2} k R_0^2 \ln \left(1 - \left(\frac{r}{R_0} \right)^2 \right) & \text{if } r < R_0 \\ \infty & \text{if } r \geq R_0 \end{cases} \quad (7)$$

Here, we take the common choice of $k = 30\epsilon_{\text{LJ}}/\sigma^2$ and $R_0 = 1.5\sigma$ for the spring constant and maximum extend of the bond, respectively. The parameters of the potential are selected that bond crossing is suppressed. For the interactions between the same type of particles (monomers, CNS), the LJ potential is shifted and truncated at a cutoff radius $r_c = 2^{1/6}\sigma$, which leads to repulsive interactions, thus implementing almost athermal solvent conditions for all components. To simulate the effect of preferential adsorption, the range of the interaction between monomers and CNS particles is extended to $r_c = 2.5\sigma$, while the interaction strength between these two types of particles varies in the following range: $\epsilon_{\text{CNS}} = [1.0, 1.2, \dots, 2.0]k_B T$.

We start with simulations of a pure polymer solution (in the absence of CNS) to calculate the osmotic pressure of linear homopolymers as a function of monomer concentration under good solvent conditions. To determine the isothermal equation of state (EoS), $p(c)$, we apply the Nosé–Hoover barostat for an NPT ensemble. Next, we select a pressure that leads to a polymer phase in the semidilute regime. As noted above, this regime is most interesting since translation entropy driven coexistence is suppressed and only a type II transition can occur.

To simulate a constant osmotic pressure for the polymer and a constant chemical potential for the CNS, we implement a membrane as sketched in Figure 1. This semipermeable membrane separates the simulation box into two parts: a polymer phase and a bulk cosolvent phase. The membrane consists of a two-dimensional array of LJ particles that do not interact with the cosolvent. The external osmotic pressure exerted by the membrane is due to a constant force acting on the membrane in the negative z direction in our coordinate system. We carry out our simulations using LAMMPS package.³⁴ The pressure exerted by the membrane is selected from the analysis of equation of state of the polymer to be inside the semidilute limit. We consider polymer chains with two different degrees of polymerization: $N = 60$ and $N = 120$. For the lateral extension of the simulation box we have chosen $A = L_x L_y = 22\sigma \times 22\sigma$. The size of the simulation box in the z direction, L_z , is chosen in between $192\sigma \leq L_z \leq 292\sigma$. The average radius of gyration of the polymers in the absence of CNS is chosen as the reference and is given by $R_{g0} = 4.901$ for $N = 60$ and $R_{g0} = 7.295$ for $N = 120$.

The equations of motion are integrated using a velocity-Verlet algorithm with a time step $\delta t = 0.005\tau$ and a damping coefficient $\Gamma = 1\tau^{-1}$ for the Langevin thermostat. Initially, a fixed number of CNS particles are distributed randomly all over the simulation box, and the initial configurations are equilibrated for typically $3 \times 10^5\tau$. Subsequently, the simulations are performed for a fixed attraction energy, ϵ_{CNS} , until reaching a time-invariant CNS density profile. The last 500 configurations are taken for all measurements. Equilibration is additionally checked by reaching the plateau value of the membrane position and the radius of gyration of the polymers. This procedure is repeated for each choice of the parameters ϵ_{CNS} and number of CNS in the simulation volume. The CNS concentration is varied from zero (pure solvent) to higher values up to 120000 CNS particles. The polymer volume is calculated by measuring the height of the membrane. In turn, we calculate $\langle V(p) \rangle$, where V denotes the box volume below the membrane.

3. RESULTS

3.1. Equation of State for the Polymer Solution and Determining the Semidilute Regime. Before considering the co-nonsolvency response, we verify that our model reproduces the characteristic behavior of polymer solutions in good solvent.³⁰ We start from the dilute regime performing canonical MD simulations in a cubic box with periodic boundary conditions in x and y directions, containing linear polymer chains with $N = 60$. We calculate the equation of state, $p(V)$, using the same method as in a recent work.³⁵ In Figure 3 we show the results with simulations under constant pressure exerted by the movable membrane while keeping the number of polymer chains fixed (red squares, $N = 60$). We compare our simulations with the results for $N = 100$ (blue circles) of ref 35 where a standard barostat has been applied.

To rationalize our results, we plot them in the expected scaling form:

$$\frac{pN}{ck_B T} = f_p \left(\frac{c}{c^*} \right) \quad (8)$$

where c^* denotes the overlap concentration, which we define as $c^* = \frac{v_0 N}{R_g^3} \propto N^{1-3\nu}$.³⁰ Here, v_0 denotes the volume of a Kuhn

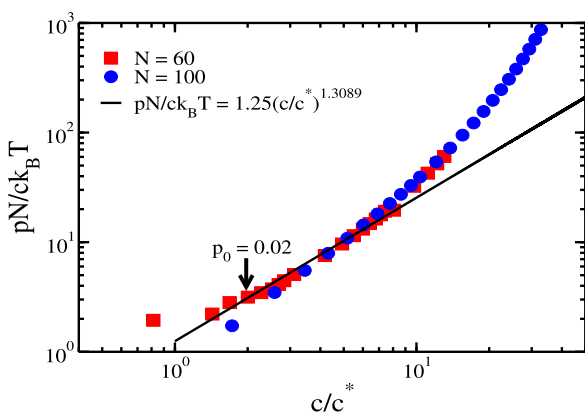


Figure 3. Concentration dependence of osmotic pressure in a good solvent for a linear polymer solution. The osmotic pressure is rescaled with respect to the ideal gas pressure, and the concentration is given in units of the overlap concentration. Simulation results are obtained in this work for $N = 60$ (red squares) and compared with the result of $N = 100$ as obtained by a standard barostat as presented in our previous work³⁵ (blue circles). The semidilute scaling regime is indicated by the black solid line. The pressure selected simulation including CNS particles is shown by an arrow. Volume and pressure are given in units of σ^{-3} and $\epsilon_{\text{LJ}}\sigma^{-3}$, respectively.

segment, and R_g is the radius of gyration of a polymer in a dilute solution which follows the scaling law $R_g \propto N^\nu$, where ν is the Flory exponent. We use $v_0 = (4\pi/3)(\sigma/2)^3$ and find $c^* = 0.043$ for $N = 60$ in a good solvent. In the dilute limit the ideal gas behavior is expected, i.e., $f_p = 1$ for $c \ll c^*$. In the asymptotic limit of $c \gg c^*$ we expect a power law behavior according to $\frac{pN}{ck_B T} \propto \left(\frac{c}{c^*}\right)^{1/(3\nu-1)}$. This is indicated by the black solid line in Figure 3 using $\nu = 0.588$. Our results agree with our previous work using a standard barostat instead of a moving membrane in ref 35, and we can clearly identify the onset of the semidilute regime. The data which is indicated by the arrow in Figure 3 corresponds to $p_0 = 0.02$, and this was selected for all CNS simulations in the rest of this work.

3.2. Polymer Solution in the Presence of CNS Particles. The actual parameter space in the presence of CNS is already very large. We are interested in the co-nonsolvency effect in the semidilute range using only a single representative pressure value of p_0 . Furthermore, the chain length effect is of minor importance in the semidilute range, and we use $N = 60$ for most of the results presented in this work. The crucial parameters are therefore the monomer–CNS interaction parameter, ϵ , in eqs 3 and 4, which is set by the simulation parameter ϵ_{CNS} , and the bulk volume fraction of CNS particles, ρ , which are added to the whole simulation box while the membrane is held under constant pressure, p_0 . To compare our simulation results with the theoretical model derived for ideal solubility of the CNS, we use the lattice-gas relation (eq 1). Typical snapshots of the simulations at different CNS concentrations using the interaction parameter $\epsilon_{\text{CNS}} = 1.8$ are shown in Figure 4. Visible is a collapse–reentry behavior of the polymer volume with respect to the amount of CNS in the simulation. A low concentration of CNS leads to a condensed polymer–CNS phase, while higher concentrations once more give rise to dissolution. This reflects the idea of the theory presented above where bridging effects dominate at low CNS concentrations, while at higher concentrations the chains

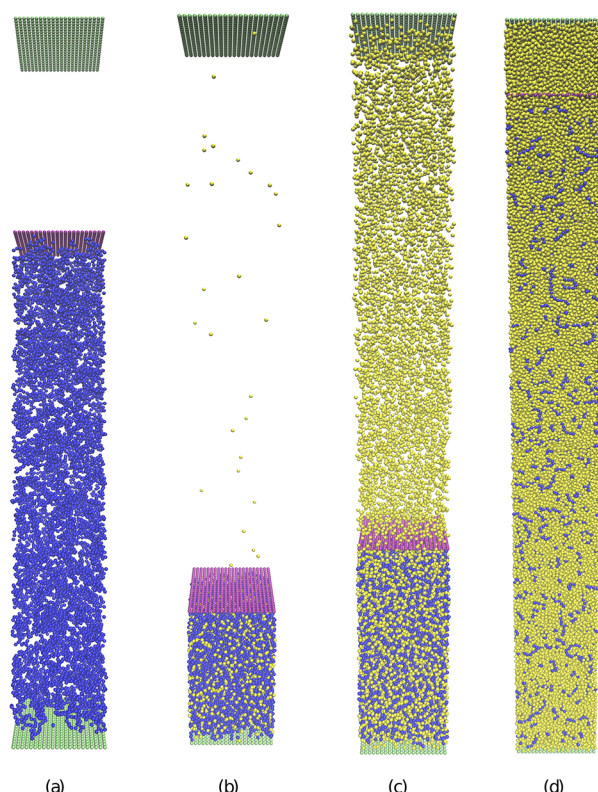


Figure 4. Snapshots of polymer solution in the presence of CNS at different concentrations of the CNS as indicated in the figures. From left to the right, the number of CNS particles increases while the number of polymers and osmotic pressure are constant. The blue color indicates polymer chains, the yellow color is used for CNS, the purple color shows the semipermeable membrane, and the green color represents impenetrable walls. The CNS–monomer interaction is set to $\epsilon_{\text{CNS}} = 1.8$. The chemical potential μ and volume fraction of CNS particles from left to the right are respectively (a) no-CNS; (b) -8.53 , 0.021 ; (c) -2.93 , 0.095 ; and (d) -0.25 , 0.507 .

are coated by CNS and finally fully dissolved in the better solvent.

In Figure 5, we display the volume of the polymer solution under constant pressure, V , as a function of the chemical potential of CNS for different interaction energies. The volume is normalized by the volume of the solution for $\rho = 0$, V_0 . Open

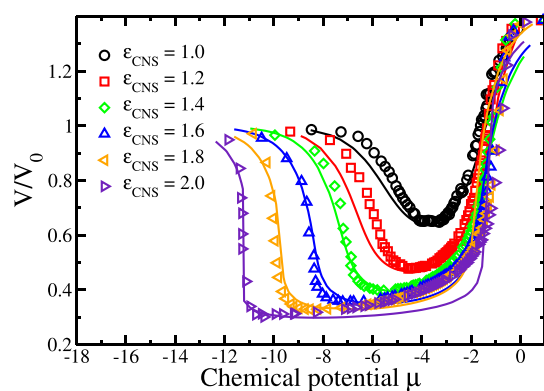


Figure 5. Normalized polymer volume is displayed versus chemical potential μ of the CNS. The osmotic pressure in the simulation is $p_0 = 0.02(\epsilon_{\text{CNS}}/\sigma^3)$, and $N = 60$ for various attractive interactions, ϵ_{CNS} , between CNS and monomers.

symbols are used to display the simulation results, and solid lines are used to show the numerical solution of our mean-field theory. The fingerprint of the co-nonsolvency transition is the nonmonotonous behavior of polymer density/polymer volume under continuous increase of the volume fraction of CNS which can be seen for all interaction parameters. The volume response of the semidilute solution is very similar to the height response of a polymer brush.²⁷ There is a minimum for each interaction energy which shifts to the lower chemical potentials as interaction energy increases corresponding to the theory outlined in section 2.1. This state is given by the maximum of the coupling which leads to $\mu \simeq -\epsilon$. The marked asymmetry of the condensation and reentry (resolvation) behavior is due to the parameter ν , which stands for the additional excluded volume of the chains due to adsorbed CNS. This additional excluded volume eventually leads to the state of the polymer under better solvent conditions, i.e., $V(\rho = 1) > V(\rho = 0) = V_0$.

With regard to the numerical solution, the simulation parameter ϵ_{CNS} has to be mapped to the adsorption energy ϵ in the mean-field model. The result is displayed in Figure 6. The

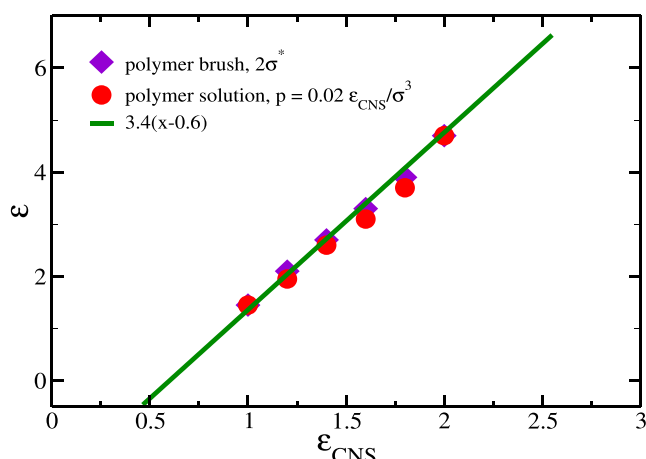


Figure 6. Mapping of the interaction parameter obtained from simulation, ϵ_{CNS} , to the mean-field model, ϵ . We include our results obtained for the co-nonsolvency response in polymer brushes taken from ref 27. The best fit for the model parameter is obtained by numerically minimizing the free energy of the polymer solution in eq 2. The grafting density of the polymer brush was 2 times the overlap density.

best fit for this mapping is given by $\epsilon = a(\epsilon_{\text{CNS}} - \epsilon_c)$. This result corresponds exactly to the one obtained for the analysis of the CNS response of polymer brushes in ref 27. The offset value of ϵ_c corresponds to the entropic barrier which emerges if a CNS molecule is adsorbed by the chain backbone.

Actually, a monotonous behavior of $V(\mu)$ is obtained for $\epsilon < \epsilon_c$, corresponding to the absence of the adsorption–attraction effect. In this case the entropic loss of a CNS particle when it is in contact with a polymer is no more compensated by the attraction between the two species. As attraction exceeds ϵ_c , the volume transition is stronger and is shifted to smaller chemical potentials. For values of $\epsilon_{\text{CNS}} > 1.6$ a jumplike collapse transition of the polymer volume is observed. We note the very good quantitative agreement of the mean-field model with the simulations in the range of the condensation transition. As in the case of polymer brushes, the quantitative agreement is less good in the reentrance region, particularly at stronger polymer–CNS attractions. The larger discrepancy of

the model prediction with respect to the simulation results for high concentrations of cosolvent is in part related to the fact that the better solvent quality of the pure cosolvent is taken into account only by the additional excluded volume contribution due to the coating of the polymer by cosolvent, given by the expression $\nu\phi$ in eq 5. In addition, an explicit Flory interaction parameter for the cosolvent/polymer interactions can be introduced to improve the quantitative agreement there.²⁹ However, we note that in most scenarios of application of the co-nonsolvency effect the collapse/condensation transition is of interest as well as a low concentrations of cosolvent. Beyond this aspect we emphasize that correlation effects due to locally higher concentrations of monomers are not taken into account in the mean-field approach in eq 4.

Conformational Properties of Individual Chains. In Figure 7a, we display the radius of gyration R_g of the polymer chains rescaled by its value in the absence of CNS, R_{g0} , versus the chemical potential μ of the CNS. The behavior of the individual chains in the semidilute state follows the signature of the CNS transition of the solution. This can be directly seen by comparing with the results for the polymer density in Figure 7c. In particular, the sharp condensation transition is reflected by a sharp collapse of the individual chains. To analyze the origin of the behavior of the individual chains, we display the results of the radius of gyration versus the monomer concentration in a parametric plot in Figure 7b. Here, the concentration is rescaled by the overlap value as defined below eq 8. As a result, we obtain a perfectly smooth behavior with two branches belonging to the condensation and the reentry regime.

This suggests that the origin of the chain collapse at the condensation transition is a consequence of the increased excluded volume screening which can be described by the well-known semidilute scaling according to $R_g \sim c^{(2\nu-1)/2(1-\nu)} \sim c^{-1/8}$, where we used Flory's result for $\nu \simeq 3/5$ in the last expression.³⁰ To test this idea, in Figure 7d we therefore displayed the radius of the gyration normalized by the expected concentration scaling, i.e., $R_g c^{1/8}$. A nearly horizontal behavior is shown in the condensation region up to the condensed state which are shown by dashed lines. This is followed by a constant increase of the radius of gyration with respect to the reference value of the semidilute state. The latter behavior can be attributed to the increase of the excluded volume, i.e., solvent quality, by increasing the CNS concentration due to a larger number of adsorbed CNS in the reentry region. This corresponds to our theoretical model, particularly to the contribution $\nu\phi$ in eq 5, which takes into account the additional excluded volume due to the adsorption of cosolvent. Thus, our analysis shows that the co-nonsolvency driven condensation transition can be described by a collective phase transition which affects the size of the polymers indirectly. We cannot find any indication for chain collapse by strong intramolecular effects due to CNS bridging. Thus, we can conclude that interchain contacts are dominating the cosolvent-induced attraction between monomers and the coupling term in the free energy given in eq 4. This, in turn, justifies the mean-field approach used in the adsorption–attraction model.

Single Chain Structure Factor. The structure factor contains information about the spatial correlations between the monomers via Fourier transform of density correlation

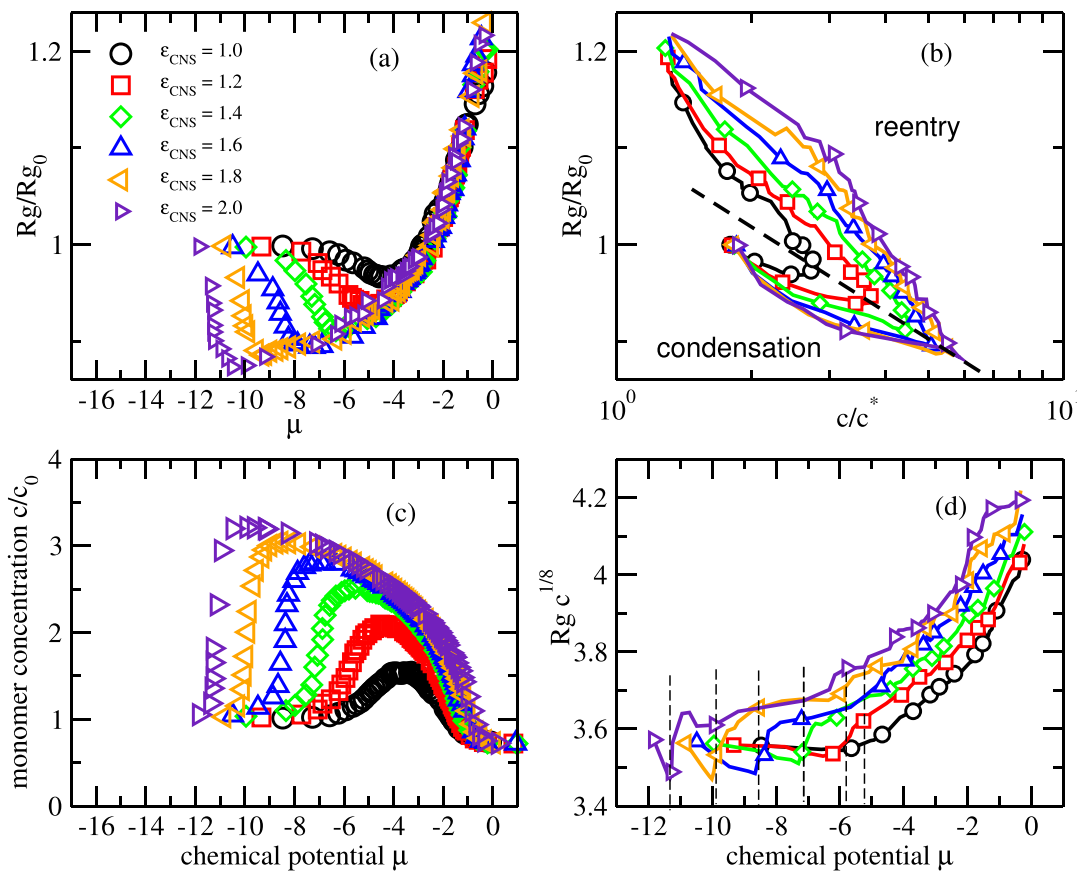


Figure 7. Analysis of the radius of gyration during condensation and reentry for various values of the interaction parameter. Part a displays the normalized values, R_g/R_{g0} , vs chemical potential of the CNS. The change of the size of the polymers follow the signature of the monomer concentration c/c_0 shown in part c where c_0 denotes the monomer concentration in the absence of CNS. In part b, we show the parametric representation of the rescaled radius of gyration and the density, c , in units of the overlap density, c^* . Here, the dashed line divides the condensation and the reentry region: Data points below the dashed line belong to the condensation regime. In part d, we present the rescaled radius of gyration $R_g c^{1/8}$ according to the expectation for the semidilute solution as a function of chemical potential of CNS in the reservoir μ . The dashed lines denote the condensation regime. All plots show simulation results for different interaction energies as noted in (a) and $N = 60$.

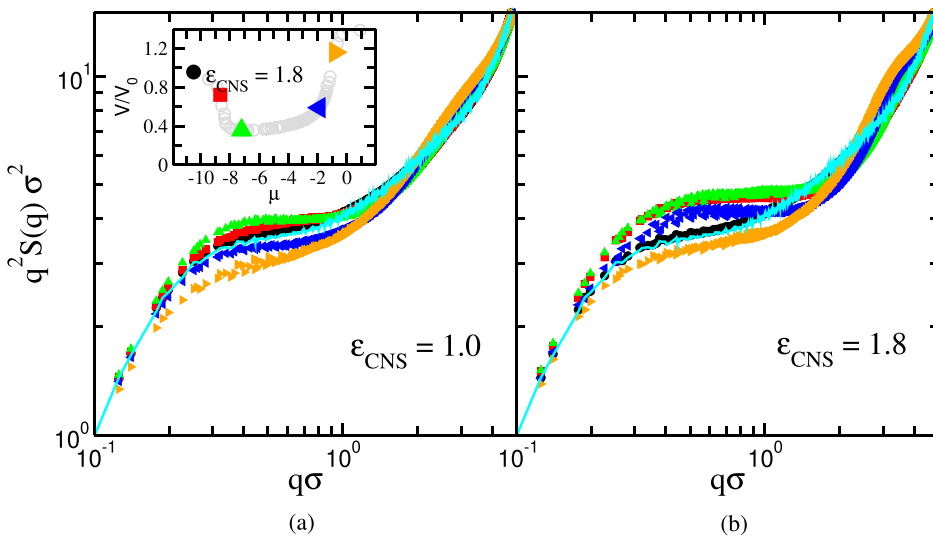


Figure 8. Kratky plot of the single chain structure factor, $S(q)$, plotted against q (in units of $1/\sigma$) for chain length $N = 120$ at different CNS concentrations for two different interaction energies: $\epsilon_{CNS} = 1.0$ and 1.8. The color/symbol code is indicated in the inset. The inset shows the data for the volume vs chemical potential for the case of $\epsilon_{CNS} = 1.8$. The cyan data (line) correspond to the semidilute solution in the absence of CNS.

functions. We are interested in the structure factor $S(q)$ of a single chain

$$S(q) = \frac{1}{N} \left\langle \sum_{m=1}^N \sum_{n=1}^N e^{i\vec{q} \cdot (\vec{r}_m - \vec{r}_n)} \right\rangle_{lq,t} \quad (9)$$

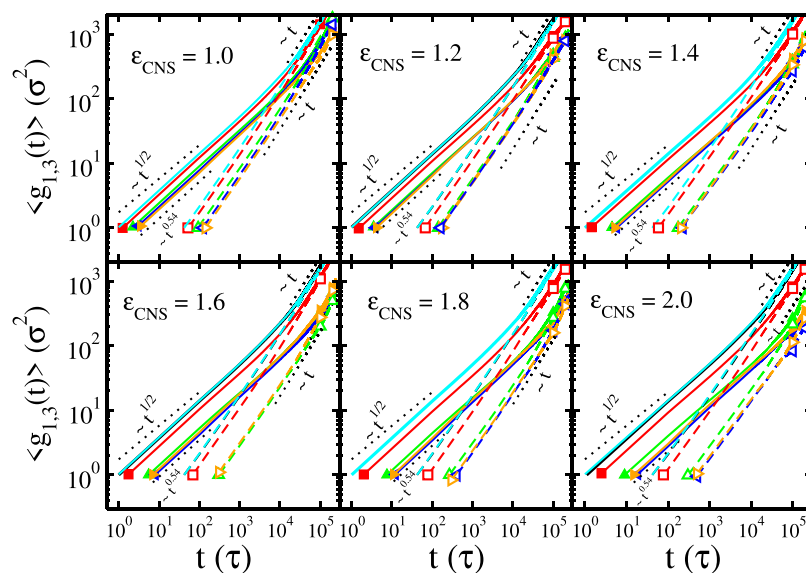


Figure 9. Dynamic functions g_1 (solid lines) and g_3 (dashed lines) for chains with length $N = 120$ as a function of time for different CNS concentrations and interaction energies. The color/symbol code for the various concentrations of CNS is taken from the inset of Figure 8. Results in the absence of CNS are drawn in cyan (no symbols). The dotted lines indicate the expected exponents in the corresponding scaling regions.

The angular brackets indicate averaging over time, orientation of wave vectors, and all chains in the solution.

In Figure 8, we display the rescaled single chain structure factor for chains of length $N = 120$ at various stages of the CNS response for two different values of the CNS–monomer interaction in a double-logarithmic representation. Most interesting is the plateau behavior which corresponds to the length scales between the Kuhn length and the radius of gyration and can be denoted as the scaling region. Lower q values, i.e., $q \ll 1/R_g$, give rise to constant scattering; thus, $q^2 S(q) \sim q^2$, while larger q values, i.e., $q \gg 1/l_b$, resolve monomer details. In our simulation model the Kuhn length is not much larger as the bead size, σ . For ideal chains, the plateau region should be horizontal, i.e., $q^2 S(q) \sim \text{const}$, while for excluded volume conditions a finite slope according to $q^{2-1/\nu} \simeq q^{1/3}$ is predicted. The inset displays again the results for the volume of the polymer solution under osmotic pressure and indicates the various stages of the CNS response for $\epsilon_{\text{CNS}} = 1.8$. The highlighted symbols define the color code in the main plots (CNS concentration). In addition, cyan color (no symbol) indicates the case of the polymer solution without CNS.

We can observe a nonmonotonous behavior of the single chain scattering with respect to the increase of the concentration of the CNS. We note that the data we have selected from the equation of state (see Figure 3) are at the beginning of the semidilute region. Thus, the plateau is dominated by excluded volume scaling in the absence of CNS. The same can be seen for the data in the CNS-dominated state (orange/triangle-right data). Because of the fact the CNS is the better solvent, the scaling region is a bit broader here. Most remarkable is the transition toward ideal scaling in the condensed state. This is in full agreement with the theoretical expectation because this state is much closer to the concentrated regime; thus, excluded volume effects are screened efficiently. At the beginning of the reentry region (blue/triangle-left data), this trend is inverted again. These results confirm our analysis of the radius of gyration described above: The statistics of the individual chains follow the change

in the polymer concentration due to the CNS effect but do not display any unusual intrachain correlation effects.

Dynamic Properties. It is an interesting question in how far the CNS effect influences the dynamics of the polymers. We note that the value of the attractive interactions between CNS and monomers, ϵ , is in the range of one and a few $k_B T$. Thus, only weak and very transient binding induced by the CNS bridges can be expected, and thus the Rouse dynamics of polymer solutions should be the reference to discuss the simulation results below. Following earlier studies of polymer dynamics in simulations, we define the following dynamic observables:

- The mean-squared displacement (MSD) of all monomers is denoted by $g_1(t)$ at time $t = n_t \Delta t$ and is calculated as

$$g_1(t) = \left\langle \frac{1}{N_t - n_t} \sum_{n_s=1}^{N_t - n_t} [\vec{r}((n_t + n_s)\Delta t) - \vec{r}(n_s\Delta t)]^2 \right\rangle_{N_m} \quad (10)$$

where $\vec{r}(t)$ is the position of each monomer at time t . The brackets denote the average over all monomer, N_m . To improve the statistics, we average over all time intervals of length n_t out of the totally available conformations, N_t .

- The MSD of all monomers with respect to the polymer's center of mass:

$$g_2(t) = \left\langle \frac{1}{N_t - n_t} \sum_{n_s=1}^{N_t - n_t} [\Delta \vec{r}((n_t + n_s)\Delta t) - \Delta \vec{r}(n_s\Delta t)]^2 \right\rangle_{N_m} \quad (11)$$

where $\Delta \vec{r}(t) = \vec{r}(t) - \vec{r}_{\text{cm}}(t)$ denotes the position of a monomer with respect to the polymer's center of mass at time t . The center of mass position of each polymer is given by $\vec{r}_{\text{cm}}(t) = \frac{1}{N} \sum_{i=1}^N \vec{r}_i(t)$

- The MSD of the center of mass of the chains:

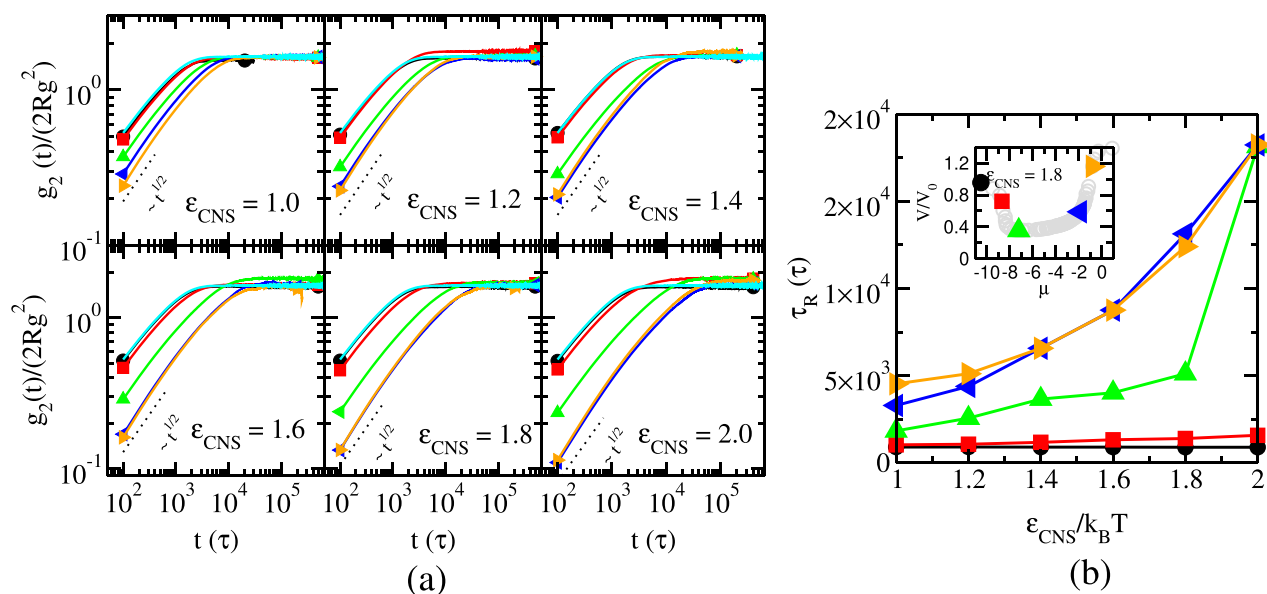


Figure 10. (a) MSD with respect to the polymer's center of mass $g_2(t)$ for a solution of linear chains in the absence (cyan/no symbols) and in the presence of CNS for polymers of length $N = 120$ as a function of time at different CNS concentrations and interaction energies. The results are normalized by $2R_g^2$. The dotted lines indicate the subdiffusive behavior as expected from the Rouse theory. (b) Rouse time τ_R as a function of interaction energy for different CNS concentrations. The inset indicates the color/symbol code.

$$g_3(t) = \left\langle \frac{1}{N_t - n_t} \sum_{n_s=1}^{N_t - n_t} [\vec{r}_{cm}((n_t + n_s)\Delta t) - \vec{r}_{cm}(n_s\Delta t)]^2 \right\rangle_{N_p} \quad (12)$$

where the average is taken over all polymers, N_p .

We denote the microscopic time scale (or monomer relaxation time) by τ_0 and the Rouse time by τ_R . The Rouse time is the longest relaxation time of unentangled polymers and scales according to $\tau_R \sim \tau_0 N^{1+2\nu}$. In the dynamic scaling regime, $\tau_0 < t < \tau_R$, the prediction of the Rouse model for $g_1(t)$ and $g_2(t)$ is given by $\sim t^{2\nu/(1+2\nu)}$, which corresponds to $t^{1/2}$ for the ideal chain and $t^{0.54}$ for good solvent condition.³⁶ At times longer than the polymer relaxation time $t > \tau_R$, normal diffusion is expected for $g_1(t) \sim t$ and $g_2(t)$ approaches a plateau. The MSD of chain's center of mass is expected to be diffusive, $g_3(t) = 2D_{cm}t$, at all the times $t > \tau_0$ where the diffusion coefficient of center of mass scales as $D_{cm} = D_0/N$, where D_0 is the monomer diffusion coefficient.

In Figure 9, we show the results of $g_1(t)$ and $g_3(t)$ for polymers of chain length $N = 120$ at different CNS concentrations and for various interaction energies. Because we apply periodic boundary conditions in the xy direction of the simulation box, we present the calculations for 2D displacements only. All plots in Figure 9 display a single crossover between subdiffusive behavior and normal diffusion. Consistently, the results for the COM diffusion display a single regime of normal diffusion. This is the signature of simple Rouse dynamics. Only in the most condensed states (green/triangle-up and blue/triangle-left) can we observe slight deviations indicating the onset of entangled dynamics (in particular, slight deviations from normal diffusion in the COM results). Therefore, the crossover between the two different scaling regimes in Figure 9 can be taken as a measure of the Rouse time. The microscopic time scale τ_0 related to the monomer relaxation time can be defined by $g_1 = \sigma^2$. The Rouse time is then defined as

$$\tau_R = N^2 \tau_0 / \pi^2 \simeq 120^2 \tau_0 / \pi^2 \simeq 1.46 \times 10^3 \tau_0 \quad (13)$$

The dashed lines are shown to compare with the expectations of the Rouse model. For time scales smaller than a Rouse time, $g_1(t)$ presents a subdiffusive behavior with exponents slightly above 0.5, which indicates that excluded volume effects still play a role particularly in the noncondensed state.

Figure 10a shows the results for $g_2(t)$ normalized by polymer's radius of gyration. Again, Rouse scaling can be observed.

To extract the Rouse time, we use the analytical expression for ideal chain dynamics:

$$g_2^i(t) = 2\alpha D_0 \tau_0 \frac{1}{N} \sum_{n=1}^{\infty} \frac{N^2}{n^2 \pi^2} (1 - e^{-n^2 \pi^2 t / N^2 \tau_0}) \quad (14)$$

The monomer diffusion constant, D_0 , is taken from the slope of the COM diffusion, $g_3(t)$, in Figure 9. The prefactor α is used as a fit parameter which expresses the difference between the ideal radius of gyration and real one. Together with adjusting τ_0 a best fit with the numerical data for $g_3(t)$ for $t \gg \tau_0$ is obtained. The Rouse time is then calculated by via eq 13.

In Figure 10b, we plot the Rouse time, τ_R , as a function of the strength of attraction between CNS and monomers and for various concentrations of the CNS in the bulk. The colors of the plots are again shown as highlighted symbols in the inset. We can observe a monotonous increase of the polymer relaxation time with respect to both the increase of the CNS–monomer attraction and also with respect to the CNS concentration. At the same time simple Rouse dynamics is displayed. The monotonous increase of the relaxation time with respect to the CNS concentration indicates the absence of network-like dynamics; i.e., the CNS effect is a rather short-living temporal attraction between monomer pairs. Otherwise, a strong increase of the relaxation time (in particular, a slowdown of the COM motion of the chains) should be observed at maximum coupling, i.e., for the maximum density of the solutions. Given our simulation results, we attribute the

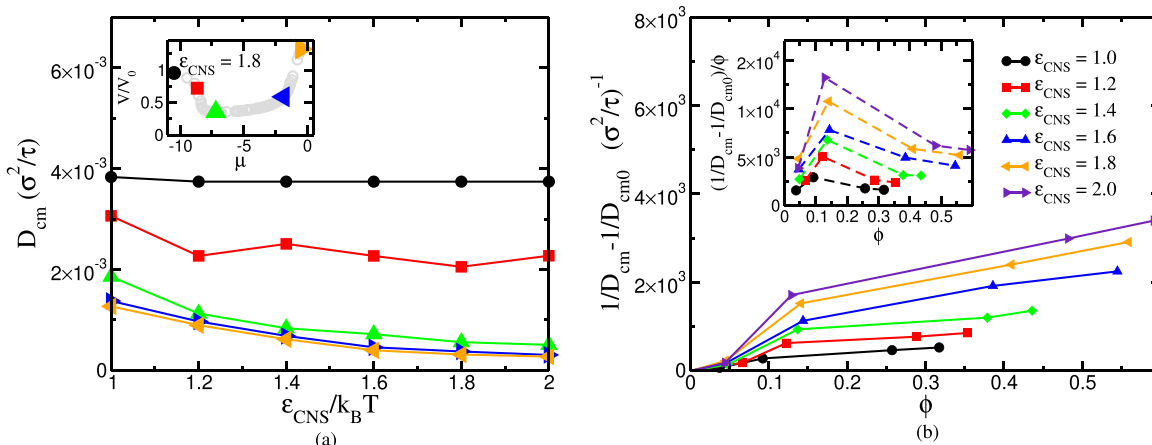


Figure 11. (a) Diffusion coefficient of the center of mass as a function of interaction energy at various concentrations of CNS (color/symbol code given in the inset). (b) Excess polymer friction coefficient due to the co-nonsolvency effect vs the order parameter for different interaction energies. Here, D_{cm0} denotes the diffusion coefficient of the COM of the chains in the absence of CNS. The inset displays the results normalized by the amount of adsorbed CNS (order parameter).

slowdown of the chain dynamics primarily to the adsorbed layer of CNS on each chain.

In Figure 11a, we present the diffusion coefficient D_{cm} of polymer's center of mass. The results of diffusion coefficients are obtained by fitting to the linear regime of $g_3(t)$ (see Figure 9). Below and also within the condensation transition (black/circle and red/square symbols) there is only weak variation with the cosolvent–monomer interaction. At higher cosolvent concentration there is a stronger but still moderate slowing down of the polymer diffusion. We note the strong but monotonous dependence on the cosolvent concentration within the condensation transition.

To investigate the effect of adsorbed cosolvent on the dynamics in more detail, we consider the polymer friction constant, i.e., the inverse of the center-of-mass diffusion constant. In Figure 11b, we display the excess polymer friction constant which we define as the difference of the polymer friction constant with respect to the friction constant in the absence of cosolvent versus the amount of adsorbed cosolvent, ϕ (order parameter, see eq 3 and below). The latter has been calculated from the simulations by taking into account cosolvent molecules that are located within the interaction range of a monomer and normalized to unity for fully saturated chains (see also ref 27). We observe a monotonous increase of the excess friction of the polymers with the amount of adsorbed cosolvent. The inset displays the same data but divided by the order parameter. Here, we can see that approximately a linear relation (plateau in the reduced plot) between the excess friction constant and the order parameter is valid except for the maximum condensed state. The latter indicates a stronger coupling between the chains, which, however, as we have seen above, does not lead to anomalous dynamics of the monomer diffusion. We note that besides the loading of chains with adsorbed CNS, the increasing amount of explicit solvent increases the friction constant as well. To rationalize the diffusion of polymers in the presence of the adsorbing cosolvent or cosolute, one needs to take into account the adsorption–desorption dynamics into the equation of motion. Of relevance will be the time scale during which an adsorbed particle will rest on the chain before desorption occurs, in particular in comparison the monomer relaxation time and the Rouse/Zimm time of the chain.

4. DISCUSSION AND CONCLUSIONS

In this work we have studied the co-nonsolvency response of a semidilute polymer solution using coarse-grained molecular dynamics simulations with an implicit common solvent. In the simulation model we assume a preferential interaction between the explicitly simulated cosolvent and the monomers. The latter is realized by an attractive interaction parameter between the two species of the order of $k_B T$. Using a semipermeable wall, we simulated the polymer phase under constant osmotic pressure in equilibrium with a bulk cosolvent phase. This enables us to study the condensation transition as a function of the bulk cosolvent concentration by measuring the volume of the polymer phase. In agreement with the adsorption–attraction model for polymer solutions, we obtain a jump-like condensation transition of the semidilute polymer phase. This transition is followed by a re-entry transition at higher cosolvent concentrations. This behavior is in full analogy with the one obtained for polymer brushes in a previous work. The observed discontinuous condensation transition in the semidilute state indicates a type II transition scenario as predicted by the adsorption–attraction model. By investigating the single chain properties, we find that the conformations of individual chains follow the semidilute concentration scaling with an increased excluded volume at higher cosolvent concentrations. The latter is due to the higher amount of adsorbed cosolvent and eventually the better solubility of the polymer in the pure cosolvent. We do not find any indication of unusual intrachain correlations due to the co-nonsolvency effect in the single-chain scattering functions. This indicates that the coupling effect due to the cosolvent is dominated by the interchain contacts in the semidilute state.

Finally, we have studied the co-nonsolvency response of the diffusion dynamics of the monomers and the chains. Given the relatively short chains in our simulations (up to 120 monomer units) in the semidilute state, we observe Rouse dynamics for all regimes of the cosolvent concentrations and interactions. Only a slight indication of entangled dynamics may be concluded from the data in the maximum condensed state. The polymer relaxation time displays a monotonously increasing behavior with respect to the cosolvent concentration also during the jump-like response of the polymer concentration at the condensation transition. We find no indication

for an anomalous network-like slowing down in the condensed state. This is in agreement with the fact that the coupling between cosolvent and monomers is of the order of a few $k_B T$. In particular, the polymer friction constant displays a nearly linear behavior with respect to the amount of adsorbed cosolvent. The loading of the chains with adsorbed cosolvent in addition with an increasing fraction of explicit cosolvent is the apparent origin of the continuous slowing down of the polymer dynamics by the co-nonsolvency effect. Merely the excess friction coefficient with respect to state in the absence of cosolvent shows a small peak at the maximum condensed state, which indicates a weak dynamical coupling between the chains. The latter is consistent with the onset of entangled dynamics. The dynamic results underline the collective nature of the co-nonsolvency transition due to preferential interaction between cosolvent and monomers in polymer solutions. In particular, the preferential interaction model does not lead to anomalous or even frozen dynamics in the condensed state.

AUTHOR INFORMATION

Corresponding Authors

Zahra Mohammadyarloo — Leibniz-Institute fur Polymerforschung Dresden, Institute Theory of Polymers, 01069 Dresden, Germany; Institute for Theoretical Physics, TU Dresden, 01069 Dresden, Germany; Phone: +49 351 4658 750; Email: mohammadyarloo@ipfdd.de; Fax: +49 351 4658 752

Jens-Uwe Sommer — Leibniz-Institute fur Polymerforschung Dresden, Institute Theory of Polymers, 01069 Dresden, Germany; Institute for Theoretical Physics, TU Dresden, 01069 Dresden, Germany; Cluster of Excellence Physics of Life, TU Dresden, 01307 Dresden, Germany;  orcid.org/0000-0001-8239-3570; Phone: +49 351 4658 750; Email: sommer@ipfdd.de; Fax: +49 351 4658 752

Complete contact information is available at:

<https://pubs.acs.org/10.1021/acs.macromol.2c01280>

Notes

The authors declare no competing financial interest.

ACKNOWLEDGMENTS

We thank H. Merlitz, J. Paturej, M. Koch, and R. Dockhorn for fruitful discussions and J. Paturej and H. Merlitz for critically reading the manuscript. J.U.S. acknowledges financial support by the Deutsche Forschungsgemeinschaft (DFG) within the project SO 277/17. J.U.S. was supported by the DFG under Germany's Excellence Strategy EXC 2068-390729961 Cluster of Excellence Physics of Life of TU Dresden. The authors thank the ZIH of the TU Dresden for providing computational resources.

REFERENCES

- (1) Winnik, F. M.; Ringsdorf, H.; Venzmer, J. Methanol-water as a co-nonsolvent system for poly (N-isopropylacrylamide). *Macromolecules* **1990**, *23*, 2415–2416.
- (2) Scherzinger, C.; Schwarz, A.; Bardow, A.; Leonhard, K.; Richtering, W. Cononsolvency of poly-N-isopropyl acrylamide (PNIPAM): Microgels versus linear chains and macrogels. *Curr. Opin. Colloid Interface Sci.* **2014**, *19*, 84–94.
- (3) Shultz, A. R.; Flory, P. Polymer Chain Dimensions in Mixed-Solvent Media. *J. Polym. Sci.* **1955**, *15*, 231.
- (4) Kiritoshi, Y.; Ishihara, K. Molecular recognition of alcohol by volume phase transition of cross-linked poly (2-methacryloyloxyethyl phosphorylcholine) gel. *Sci. Technol. Adv. Mater.* **2003**, *4*, 93–98.
- (5) Zhang, Q.; Hoogenboom, R. Polymers with upper critical solution temperature behavior in alcohol/water solvent mixtures. *Prog. Polym. Sci.* **2015**, *48*, 122–142.
- (6) Yong, H.; Bittrich, E.; Uhlmann, P.; Fery, A.; Sommer, J.-U. Co-Nonsolvency Transition of Poly(N-isopropylacrylamide) Brushes in a Series of Binary Mixtures. *Macromolecules* **2019**, *52*, 6285–6293.
- (7) Tanaka, F.; Koga, T.; Winnik, F. M. Temperature-Responsive Polymers in Mixed Solvents: Competitive Hydrogen Bonds Cause Cononsolvency. *Phys. Rev. Lett.* **2008**, *101*, 028302.
- (8) Tanaka, F.; Koga, T.; Kojima, H.; Xue, N.; Winnik, F. M. Preferential Adsorption and Co-nonsolvency of Thermoresponsive Polymers in Mixed Solvents of Water/Methanol. *Macromolecules* **2011**, *44*, 2978–2989.
- (9) Okada, Y.; Tanaka, F. Cooperative Hydration, Chain Collapse, and Flat LCST Behavior in Aqueous Poly(N-isopropylacrylamide) Solutions. *Macromolecules* **2005**, *38*, 4465–4471.
- (10) Mukherji, D.; Kremer, K. Coil-Globule-Coil Transition of PNIPAm in Aqueous Methanol: Coupling All-Atom Simulations to Semi-Grand Canonical Coarse-Grained Reservoir. *Macromolecules* **2013**, *46*, 9158.
- (11) Mukherji, D.; Marques, C. M.; Kremer, K. Polymer collapse in miscible good solvents is a generic phenomenon driven by preferential adsorption. *Nat. Commun.* **2014**, *5*, 4882.
- (12) Mukherji, D.; Marques, C. M.; Stuehn, T.; Kremer, K. Co-nonsolvency: Mean-field polymer theory does not describe polymer collapse transition in a mixture of two competing good solvents. *J. Chem. Phys.* **2015**, *142*, 114903.
- (13) Heyda, J.; Muzdalo, A.; Dzubiella, J. Rationalizing Polymer Swelling and Collapse under Attractive Cosolvent Conditions. *Macromolecules* **2013**, *46*, 1231–1238.
- (14) Coalson, R. D.; Nasrabad, A. E.; Jasnow, D.; Zilman, A. A Polymer-Brush-Based Nanovalve Controlled by Nanoparticle Additives: Design Principles. *J. Phys. Chem. B* **2015**, *119*, 11858–11866.
- (15) Opferman, M. G.; Coalson, R. D.; Jasnow, D.; Zilman, A. Morphological control of grafted polymer films via attraction to small nanoparticle inclusions. *Phys. Rev. E* **2012**, *86*, 031806.
- (16) Saha, S.; Weber, C. A.; Nousch, M.; Adamo-Arana, O.; Hoege, C.; Hein, M. Y.; Osborne-Nishimura, E.; Mahamid, J.; Jahnel, M.; Jawerth, L.; Pozniakowski, A.; Eckmann, C. R.; Jülicher, F.; Hyman, A. A. Polar Positioning of Phase-Separated Liquid Compartments in Cells Regulated by an mRNA Competition Mechanism. *Cell* **2016**, *166*, 1572–1584.
- (17) Sandholtz, S. H.; MacPherson, Q.; Spakowitz, A. J. Physical modeling of the heritability and maintenance of epigenetic modifications. *Proc. Natl. Acad. Sci. U. S. A.* **2020**, *117*, 20423–20429.
- (18) Sommer, J.-U.; Merlitz, H.; Schiessl, H. Polymer-Assisted Condensation: A Mechanism for Hetero-Chromatin Formation and Epigenetic Memory. *Macromolecules* **2022**, *55*, 4841–4851.
- (19) Dudowicz, J.; Douglas, J. F.; Freed, K. F. Mixtures of two self- and mutually-associating liquids: Phase behavior, second virial coefficients, and entropy-enthalpy compensation in the free energy of mixing. *J. Chem. Phys.* **2017**, *147*, 064909.
- (20) Zhang, G.; Wu, C. Reentrant coil-to-globule-to-coil transition of a single linear homopolymer chain in a water/methanol mixture. *Physical review letters* **2001**, *86*, 822.
- (21) Bharadwaj, S.; Niebuhr, B.-J.; Nothdurft, K.; Richtering, W.; van der Vegt, N. F. A.; Papadakis, C. M. Cononsolvency of thermoresponsive polymers: where we are now and where we are going. *Soft Matter* **2022**, *18*, 2884–2909.
- (22) Sommer, J.-U. Adsorption-Attraction Model for Co-Nonsolvency in Polymer Brushes. *Macromolecules* **2017**, *50*, 2219–2228.
- (23) Sommer, J.-U. Gluonic and Regulatory Solvents: A Paradigm for Tunable Phase Segregation in Polymers. *Macromolecules* **2018**, *51*, 3066–3074.
- (24) De Gennes, P.-G. A second type of phase separation in polymer solutions. *C. R. Acad. Sci. II* **1991**, *313*, 1117–1122.

- (25) Chen, Q.; Kooij, E. S.; Sui, X.; Padberg, C. J.; Hempenius, M. A.; Schön, P. M.; Vancso, G. J. Collapse from the top: brushes of poly(N-isopropylacrylamide) in co-nonsolvent mixtures. *Soft Matter* **2014**, *10*, 3134.
- (26) Yu, Y.; Cirelli, M.; Kieviet, B. D.; Kooij, E. S.; Vancso, G. J.; de Beer, S. Tunable friction by employment of co-non-solvency of PNIPAM brushes. *Polymer* **2016**, *102*, 372.
- (27) Galuschko, A.; Sommer, J.-U. Co-nonsolvency response of a polymer brush: A molecular dynamics study. *Macromolecules* **2019**, *52*, 4120–4130.
- (28) Baulin, V.; Zhulina, E.; Halperin, A. Self-consistent field theory of brushes of neutral water-soluble polymers. *J. Phys. Chem.* **2003**, *119*, 10977.
- (29) Yong, H.; Merlitz, H.; Fery, A.; Sommer, J.-U. Polymer Brushes and Gels in Competing Solvents: The Role of Different Interactions and Quantitative Predictions for Poly(N-isopropylacrylamide) in Alcohol–Water Mixtures. *Macromolecules* **2020**, *53*, 2323–2335.
- (30) de Gennes, P.-G. *Scaling Concepts in Polymer Physics*; Cornell University Press: Ithaca, NY, 1979.
- (31) Wang, R.; Wang, Z.-G. Theory of Polymers in Poor Solvent: Phase Equilibrium and Nucleation Behavior. *Macromolecules* **2012**, *45*, 6266–6271.
- (32) Kremer, K.; Grest, G. S. Dynamics of entangled linear polymer melts: A molecular-dynamics simulation. *J. Chem. Phys.* **1990**, *92*, 5057–5086.
- (33) Grest, G. S.; Kremer, K. Molecular dynamics simulation for polymers in the presence of a heat bath. *Phys. Rev. A* **1986**, *33*, 3628–3631.
- (34) Plimpton, S. Fast Parallel Algorithms for Short-Range Molecular Dynamics. *J. Comput. Phys.* **1995**, *117*, 1.
- (35) Paturej, J.; Sommer, J.-U.; Kreer, T. Universal equation of state for flexible polymers beyond the semidilute regime. *Physical review letters* **2019**, *122*, 087801.
- (36) Rubinstein, M.; Colby, R. H. *Polymer Physics*; Oxford University Press: New York, 2003; Vol. 23.